

In situ poly(ethylene terephthalate) microfibers- and shear-induced non-isothermal crystallization of isotactic polypropylene by on-line small angle X-ray scattering

Zhong-Ming Li*, Liangbin Li, Kai-Zhi Shen, Ming-Bo Yang, Rui Huang

State Key Laboratory of Polymer Materials Engineering, College of Polymer Science and Engineering, Sichuan University, Chengdu, Sichuan 610065, People's Republic of China

Received 21 October 2004; received in revised form 20 February 2005; accepted 9 April 2005

Available online 28 April 2005

Abstract

In situ microfibrillar reinforced blend (MRB) based on poly(ethylene terephthalate) (PET) and isotactic polypropylene (iPP) was elaborated by a slit die extrusion, hot stretching, and quenching process. The scanning electronic microscopic images show well-developed PET microfibers in the blends. The on-line small angle X-ray scattering (SAXS) test shows that PET microfibers have high nucleation for iPP crystallization. At the same time, after shear, neat iPP and microfibrillar blend both can faster crystallization rate. Three nucleation origins are proposed in microfibrillar reinforced blends under shear flow field: (a) the classical row nuclei model, (b) fiber nuclei and (c) nuclei induced by fiber assistant alignment. The polarized optical microscopic images indicate that, during the non-isothermal crystallization at a cooling rate of 10 °C/min from 200 °C to room temperature, the neat iPP forms common spherulites, while the diluted microfibrillar blend with 1 wt% of PET has a typical transcrystalline structure.

© 2005 Elsevier Ltd. All rights reserved.

Keywords: Microfibrillar; Shear; Crystallization

1. Introduction

Blending of structurally different polymers is a versatile way to produce new materials with desirable properties. Unfortunately, most of polymer pairs are thermodynamically immiscible and technologically incompatible, and consequently form a multiphase system during processing that may deteriorate the mechanical properties of the blends. Fortunately, the shape and size of the dispersed phase in the multiphase systems can be adjusted to form tailored morphology during processing. Some morphology can enhance the mechanical properties, while some can bring out new functions, such as impermeability to solvents and oxygen. A typical example involves a new type of in situ composite, which comprises two thermoplastic polymers

having distinct difference in melting temperatures. This material is originally manufactured by the following three processing steps [1–3]: (1) melt blending of the starting neat polymers and extrusion, (2) cold drawing of the blend, and (3) subsequent annealing of the drawn blend at constant strain and at $T_1 < T < T_2$, where T_1 and T_2 are the melting temperatures of the two components, respectively. Fabrication of in situ microfibrillar blend is a promising way for recycling of waste thermoplastics such as polyester film and drink bottle, polyolefin film, pipe and commodity, etc. [4]. In previous studies [5,6], we prepared poly(ethylene terephthalate) (PET)-polyolefin (PE and iPP) microfibrillar blends via a slit die extrusion-hot stretching-quenching process, and reported the significant reinforcement of the microfibers to the blends. Generally, the ultimate properties of fiber reinforced polymer materials based on crystallizable thermoplastics are determined in part by the crystalline morphology of the polymer matrix that in turn depends on the rates of nucleation and crystal growth [7–9]. The study of the crystallization kinetics of iPP is particularly of great importance for the design of processing operations and their relation with the final polymer structure. This is because iPP

* Corresponding authors. Tel.: +86 28 8540 1988; fax: +86 28 8540 5324.

E-mail address: zm_li@263.net.cn (Z.-M. Li).

is a polymorphic polymer with a high tendency to crystallize in numerous crystal modifications and generate various crystal morphologies [10–13]. Therefore, from the view of practice, the understanding of non-isothermal crystallization kinetics for a specific crystalline material under shear and/or elongational flow fields is more important since the microstructure of the material is mainly generated in the processing stage [14,15]. We have found that PET in situ microfibrils had high nucleation ability for the crystallization of the iPP matrix phase [16]. It caused the increases of crystallization temperature and crystallization rate during non-isothermal crystallization process. Hot stretch ratio and blend composition, which are two critical parameters for generation of microfibrillar blend, also affected the

crystallization and crystal structure of iPP [17–19]. Besides, the transcrystalline morphology in the as-stretched sample was observed in the microfibrillar PET/iPP blend [19,20]. In this study, the PET microfibrils-induced non-isothermal crystallization of iPP was investigated by in situ SAXS, especially, under a shear flow field.

2. Experimental

The PET as the microfiber candidate is a commercial grade of textile polyester and is supplied in pellets by UBE Co., Japan. Its number average molecular weight (\bar{M}_n) is approximately, 2.1×10^4 g/mol. iPP as the matrix is a

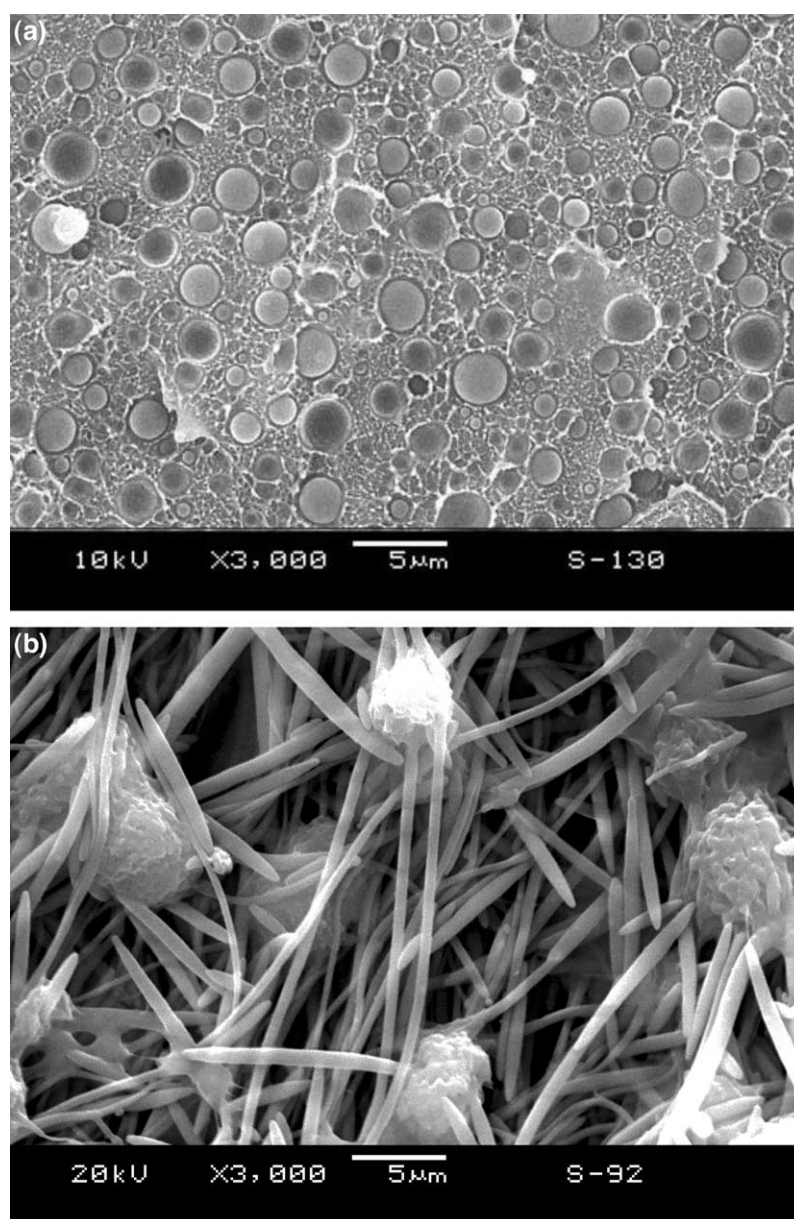


Fig. 1. SEM macrographs of (a) the cryofractured surface for the common PET/iPP (15/85 by weight) blend, and (b) the as-stretched microfibrillar PET/iPP (15/85 by weight) blend in which the PE matrix was etched by hot xylene.

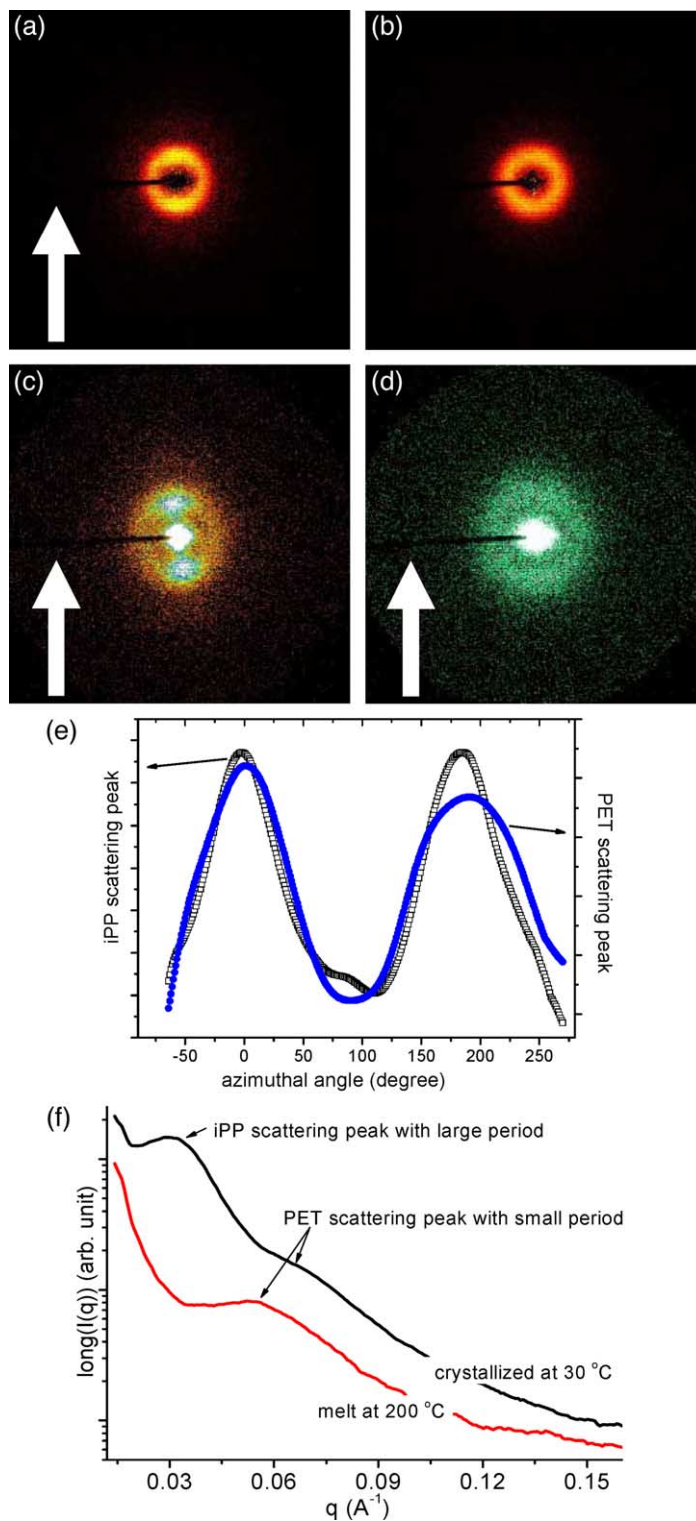


Fig. 2. (a) and (b) SAXS patterns of the as-stretched pure iPP at room temperature and 200 °C, respectively. (c) and (d) SAXS patterns of the as-stretched microfibrillar PET/iPP (15/85 by weight) blend at room temperature and 200 °C, respectively. (e) The azimuthal angle distribution of the scattering intensity of the SAXS peaks from (c) and (d). (f) The integrated one-dimensional SAXS intensity profiles versus q . $q = 4\pi \sin \theta/\lambda$, the modulus of the momentum transfer vector q , $\lambda = 0.1542$ nm being the X-ray wavelength and 2θ the scattering angle. Arrow indicates the flow direction.

commercial product (F401, Lanzhou Petroleum Chemical Co., China) with \bar{M}_n about 11.0×10^4 g/mol and melt flow index (MFI) of 2.5 g/10 min (190 °C, 21.6 N). In order to avoid hydrolysis PET was dried in a vacuum oven at 100 °C for at least 12 h prior to processing.

The detailed process of the microfibrillar blend fabrication has been described elsewhere [5]. The extrusion of the mixture of PET and iPP was performed on a single-screw extruder with a slit die. The extrudate was hot stretched by a take-up device. The line speed of the rolls was 16.0 mm/s. The roll temperature was kept at about 40 °C. Hot stretching ratio, which, by definition, is the area of the transverse section of the die to the area of the transverse section of the extrudate, is maintained at 16.1 in this study.

For scanning electron microscope (SEM) observation, the specimens were preferentially etched by hot xylene at 110 °C for 2 h. After the solvent volatilised completely, the surfaces were coated with a layer of gold and the domain morphology was observed with SEM (JEOL JSM-5900LV).

The lamellar spacing as well as their orientation was determined by small angle X-ray scattering (SAXS) measurement, which were made by using an in-house setup with a rotating anode X-ray generator (Rigaku RU-H300, 18 kW). The SAXS intensity was collected with a two-dimensional gas-filled wire detector (Bruker Hi-Star). A semitransparent beamstop placed in front of the area detector allowed monitoring the intensity of the direct beam. Details about the SAXS setup can be found elsewhere [21]. In in situ rheo-SAXS measurement, a Linkam CSS450 temperature-controlled shear system was employed as sample stage. The glass windows were replaced by two brass plates with apertures covered by 50 μm thick Kapton foil for the X-ray beam. The sample was held in the gap

between the two windows and sheared by a single rotation step of the bottom plate. The samples were preshaped into thin disks with a thickness and a diameter of about 1.2 and 30 mm, respectively. Subsequently, they were pressed between the two plates at 200 °C to a gap of 1.0 mm. After the thickness adjustment the sample was cooled and cut to fit the diameter of the upper plate. For the actual measurements the sample was first melted at 200 °C for 10 min and then cooled to 30 °C at a cooling rate of 10 °C/min. Upon cooling, a step shear was applied with a shear rate of 1 s^{-1} for 2 min at a fixed shear strain of 1500%. The whole process was monitored by SAXS using 30 s/frame.

For crystalline morphology observation, an optical polarizing microscope, Olympus BX 51 model, was used. Samples were melted and squeezed between microscopic glass at 200 °C, then put on the hot stage. The samples were maintained at 200 °C for 5 min, then non-isothermally crystallized at a cooling rate of 10 °C/min from this temperature to room temperature. In initial examination, it was found that the crystalline morphology of iPP for the undiluted blends was hard to identify. Hence, the in situ microfibrillar blend was mixed with some fresh neat iPP resin at 200 °C in the attached mixer of a Haake rheometer so that it was diluted to 1 wt% PET concentration. The phase morphology of PET can be maintained under such mixing temperature since the melting temperature of PET is much higher than 200 °C, but a new morphology is formed for the PP phase, possibly affected by the PET fibers.

Atomic force microscope (AFM) measurements were performed with a microscope from NT-MDT. Height and phase images were obtained simultaneously while operating the instrument in the tapping mode under ambient conditions. The flat surfaces for AFM measurements were obtained by cryogenic cutting at liquid nitrogen temperature.

3. Results and discussion

Fig. 1 shows the SEM micrographs of common and microfibrillar PET/iPP (15/85 by weight) blends. The common PET/iPP blend presents a typical incompatible blend morphology comprising the discrete spherical PET domains dispersed in the continuous iPP phase. No phase orientation or difference in shape of the dispersed domains is observed. Besides, no evidence suggests that any interfacial interactions or adhesion exist. Fig. 1(b) shows microfibrillar morphology, indicating PET fibers were successfully generated in situ during slit extrusion and hot stretching. The diameter of the microfibers is rather uniform (ca. 0.8 μm). Their length and aspect ratio are two crucial parameters to define the fibers, they cannot, however, be available because one cannot observe intact fibers.

It was well established that after stretching operation, the molecules have more or less orientation along the stretching direction [22,23]. In PET/iPP blend, there are two polymers

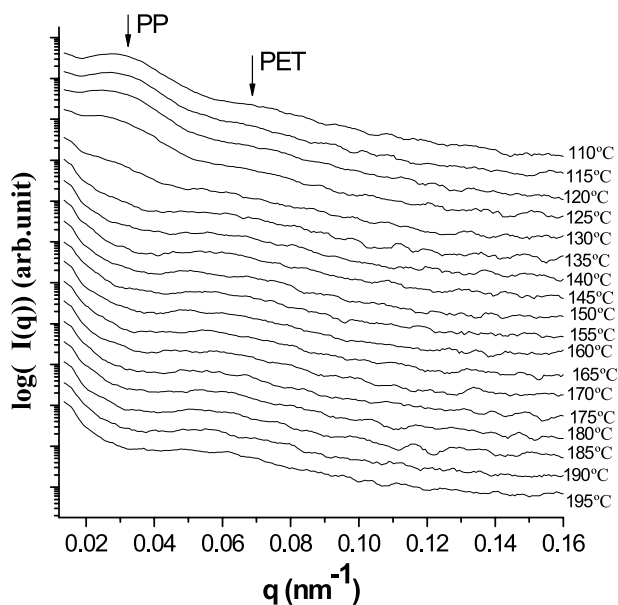


Fig. 3. One-dimensionally integrated SAXS of microfibrillar PET/iPP (15/85 by weight) blend during non-isothermal crystallization under shear at a cooling rate 10 °C/min.

with a great difference in processing temperatures (e.g. $\sim 265^\circ\text{C}$ for PET, and $\sim 190^\circ\text{C}$ for iPP), which gives an attractive point of molecular orientation. Fig. 2(a) and (c) show two-dimensional SAXS patterns of the as-stretched pure iPP and PET/iPP (15/85 by weight) blend, which reveal highly oriented lamellar crystals with layer parallel to the flow direction. In order to show the correlation between PET and iPP crystals, samples were heated up to 200°C , where only PET crystals survive and iPP is in amorphous melting state. Fig. 2(b) and (d) give the two-dimensional SAXS patterns at 200°C . As expected, PET maintains its molecular orientation, while iPP does not. The intensity distributions along with azimuthal angle from Fig. 2(c) and (d) are plotted in Fig. 2(e), which indicates iPP crystals have almost the same orientation as PET lamella. Fig. 2(f) shows the integrated SAXS intensity versus the modulus of scattering vector (q) curves of the as-stretched neat iPP and microfibrillar PET/iPP blend. There is only one clear-cut scattering peak in each curve, which is attributed to bulk iPP. The lamellar crystals of PET have a relatively short period, which present a weak peak shadowed by the high- q tail of iPP SAXS peak.

The two-dimensional SAXS intensity was integrated azimuthally to obtain the scattering profile as a function of $q = (4\pi/\lambda)\sin\theta$, the modulus of the momentum transfer vector q , λ being the wavelength and 2θ the scattering angle. Fig. 3 shows the integrated SAXS pattern of the samples during crystallization at a cooling rate of $10^\circ\text{C}/\text{min}$ from 200°C . For the sake of brevity, here only the microfibrillar PET/iPP (15/85 by weight) blend after shear is presented. It can be seen from these curves that, above 140°C , there is no clear peak that can be assigned to the crystalline region of PET (generally, the maximum crystallization rate temperature for PET at $170\text{--}180^\circ\text{C}$). When the sample is cooled to 140°C , the crystallization peak of iPP phase in the microfibrillar blend appears. With the decrease of the

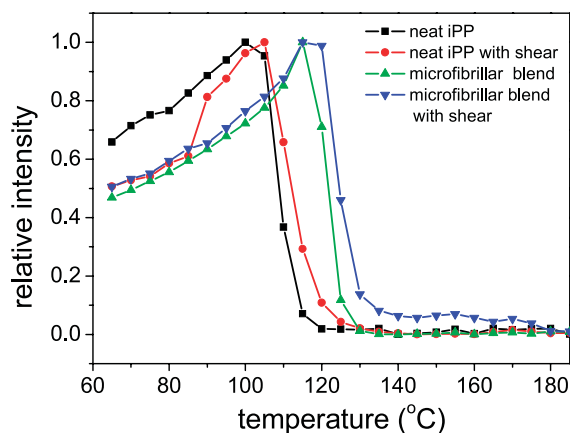


Fig. 4. Crystallization kinetics (estimated from the total scattered intensity versus crystallization temperature) of pure iPP and PET/iPP (15/85 by weight) in situ microfibrillar blend under quiescent condition and shear flow field.

temperature, the intensity of the peak becomes stronger, implying the increase of the crystallinity of the iPP.

The SAXS intensity data can be used for the determination of the crystallization kinetics of polymers [24]. At $t = 0$ (or $T =$ onset crystallization temperature for non-isothermal crystallization), the value of the total scattered intensity, $I(0)$, is due to the amorphous, non-crystalline melt. The increase in the total scattered intensity, $I(T) - I(0)$, is then directly proportional to the growth of the crystallites in the polymer. The total scattered intensity reaches a maximum, $I(s)$, at the end of crystallization. The fraction of crystallization material, $X(T)$, can be approximated as:

$$X(T) = \frac{[I(T) - I(0)]}{[I(s) - I(0)]} \quad (1)$$

Fig. 4 shows for neat iPP and microfibrillar PET/iPP (15/85 by weight) blend the variation of the $X(T)$ with temperature during cooling from 200°C with and without shear. Note that the decrease of the scattered intensity at low temperature side is due to the decrease of density contrast between the crystal and amorphous, because the intensity is proportional to the square of the difference between crystal density and amorphous density in the material. The crystallization kinetic parameters including onset crystallization temperature and half crystallization time estimated from Fig. 4 are listed in Table 1. It shows that the onset crystallization temperature for neat iPP and microfibrillar blend is, respectively, 120.2 and 130.5°C under quiescent condition, being consistent with the results from DSC [17]. It is worthy of noting that, when a step shear at the initial cooling stage was used, the onset temperature for both pure iPP and microfibrillar blend increases greatly, and reaches 130.1 and 140.6°C , respectively, indicating a significant shear-induced crystallization effect. On the other hand, while the half-crystallization time for neat iPP and microfibrillar blend agrees with that from DSC under quiescent condition, the shear crystallized samples have larger half-crystallization time than the respective quiescent crystallized ones. It indicates that though shear can induce nucleation at higher temperature, it has little effect on the crystal growth. That is, shear is more effective on nucleus formation than crystal growth.

Fiber percentage has an effect on the crystallization

Table 1
Collection of kinetic parameters for pure iPP and PET/iPP (15/85 by weight) microfibrillar blend from SAXS

Sample	T_0 ($^\circ\text{C}$)	$t_{1/2}^a$ (s)
Neat iPP		
Quiescent	120.2	65.1
Shear	130.1	87.3
PET/iPP microfibrillar blend		
Quiescent	130.5	41.9
Shear	140.6	65.7

^a $t_{1/2}$ is obtained from the relative crystallinity–crystallization time curves which were converted from Fig. 4.

kinetics of a semi-crystalline polymer composite [25]. Usually, the heterogeneously nucleated crystallization has its maximum crystallization rate at 2–6 wt% of fillers and fibers in the materials. Below the saturation value, with the increase of the fillers, the overall crystallization rate and the number of crystallites are significantly increased and crystal size reduced [26]. But the crystal growth rate is more or less decreased by truncated crystals at filler concentrations higher than the saturation value (usually 5 or 6 wt%). In previous study [19], we found that incorporation of 5 wt% PET microfibers into iPP can greatly faster crystallization of the iPP matrix, higher PET concentration, however, has little influence on the onset and maximum crystallization temperatures of the PP matrix during cooling from melt. Fig. 5 shows the effect of PET microfibers on the relative crystallinity ($X(T)$) as a function of temperature during cooling from 200 °C with and without shear. Under quiescent conditions, both blends with 5 and 15 wt% PET have almost the same crystallization kinetics. But after shear, there is an abnormal phenomenon for the blend with 5 wt% PET in that the iPP phase starts to crystallize at about 168 °C, and much faster than that with 15 wt% at above 126 °C. Apparently, too high PEC microfiber content is not in favour of iPP crystallization under shear conditions.

Numerous investigations indicate that rheo-SAXS patterns can on-line examine the evolution of the crystal structure, especially the orientated one like shish-kebab crystals [22–24]. Unfortunately, because PET phase in the microfibrillar blend already possesses certain orientation before shear as shown in Fig. 2(d), so it is impossible in the present situation to compare the crystal structures before and after shear.

It is well known that the existence of fibrillar heterogeneity or homogeneity materials can affect crystal morphology of iPP. For example, the early formation and high density of the iPP row nuclei formed along the partially carbon-coated iPP fibers lead to the formation of an apparent transcrystalline zone of the iPP in the vicinity of its precoated fiber [27,28]. We have observed typical transcrystalline layers of

iPP induced by 1 wt% PET in situ microfibers under isothermal condition [17]. Fig. 6 shows the crystalline morphology of neat iPP and microfibrillar blend obtained at a cooling rate of 10 °C/min from 200 °C to room temperature. As expected, the microfibrillar blend (Fig. 6(a)) shows a transcrystalline structure in which the transcrystalline layers fill the observed region and the PET microfibers are surrounded by the iPP crystalline layers, indicating the PET microfibers play as the center row nuclei. It should be pointed out that the microfibrillar blend for POM observation was diluted by adding some fresh PP resin and then melt mixing in a Haake mixer at 190 °C. For comparison purpose, the crystalline morphology of neat iPP was also observed, as shown in Fig. 6(b). The neat PP has a typical spherulite morphology.

The investigation of polymer crystallization from melts under the influence of a flow field (shear, elongational or combined) has drawn much interest recently because it can provide a means to predict the product morphology and properties originating from varying processes [29–31]. Varga and co-workers have shown that in pure iPP, melt-shearing caused development of row-nuclei in the form of microfibrillar bundles and promoted the epitaxial growth of folded chain lamellae that filled the space normal (perpendicular) to the row-nuclei, resulting in a supramolecular structure of cylindrical symmetry or cylindrites [32]. In contrast, quiescent melt crystallization shows only spherulitic structures with folded chain lamellae. While some in situ rheo-optical techniques have been used for observation of the flow-induced structures in the early stages of crystallization [33], the in situ rheo-SAXS and rheo-WAXD techniques turn out to be powerful methods to reveal new information on the orientation-induced structures [34,35].

In our present study, its interesting points lie in (1) comparison between in situ microfiber induced crystallization in a microfibrillar blend and the extent fibers induced crystallization in a fiber reinforced semi-crystalline polymer composite, (2) combined microfiber and shear flow induced crystallization, and (3) the origins for microfiber induced nuclei, and shear flow induced nuclei. It is apparent from the above experimental results that in situ PET microfibers and shear can both considerably induce iPP crystallization. On the other hand, the presences of both shear flow field and microfibers may lead to several kinds of nucleation origins. The hydrodynamic origin of the flow-induced orientation in polymer melt is due to the presence of entanglement, which causes the elastic extension of the chain segments between them. The chain segments between entanglement points are stretched from a state of random coil to become extended chains in the field of shear flow [36,37]. These extended chains can form some bundle-like structures, and serve as the row-nuclei. Note the row-nuclei can be a mesophase such as smectic phase instead of extended-chain crystals [35]. On the other hand, PET fibers can also induce growth of iPP crystals even without flow

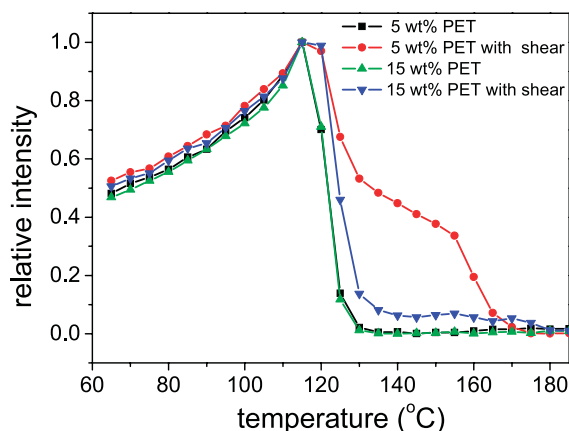


Fig. 5. Crystallization kinetics of in situ microfibrillar blends with 5 and 15 wt% of PET under quiescent condition and shear flow field.

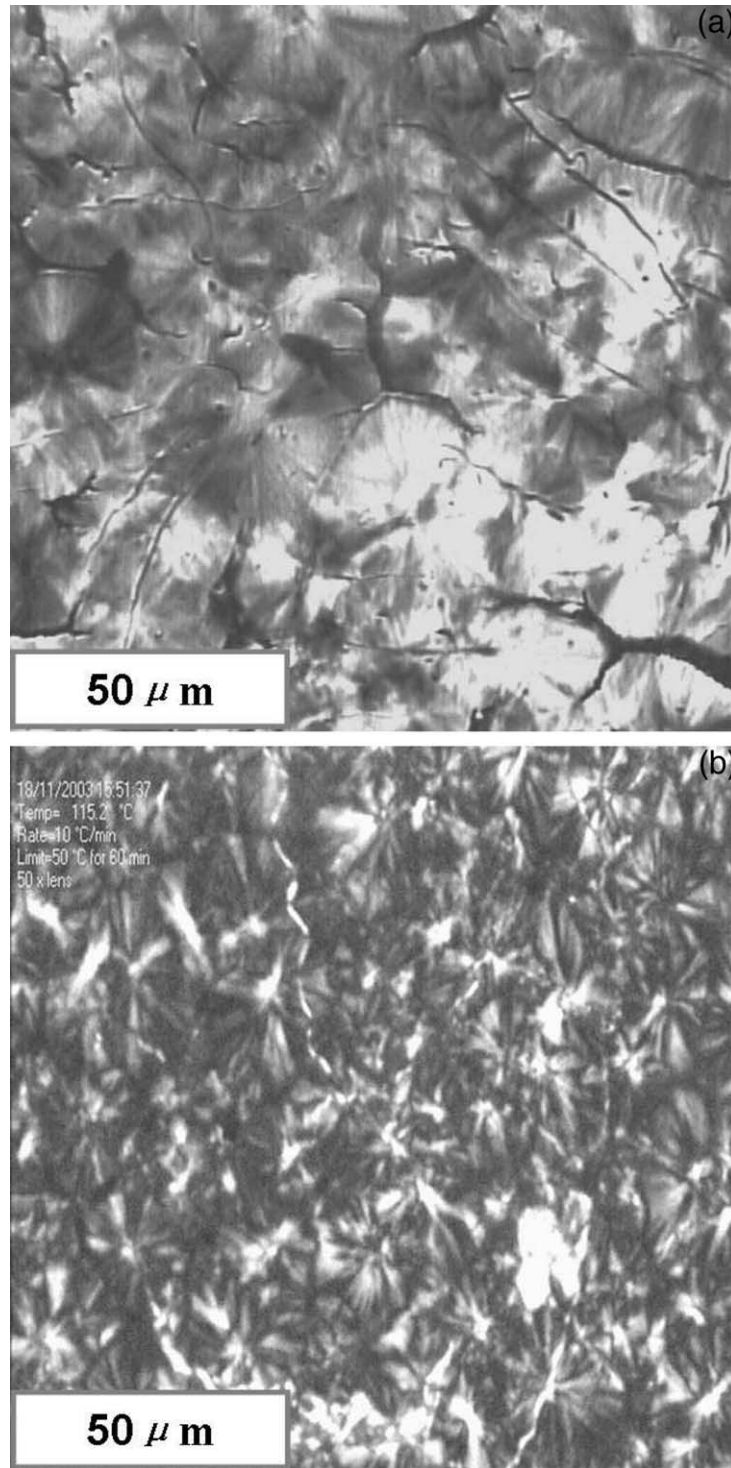


Fig. 6. Crystalline morphology of neat iPP and PET/iPP microfibrillar blend obtained by non-isothermal crystallization at a cooling rate of 10 °C/min from 200 °C to room temperature. (a) PET/iPP microfibrillar blend with 1 wt% of PET which was obtained by diluting a 15/85 PET/iPP microfibrillar blend using fresh iPP resin. (b) Neat iPP.

field as indicated by the DSC and SAXS measurement [17,18]. The presence of a surface can certainly help the alignment of molecular chains of iPP [38–41]. In our case, a shear flow field was applied to PET/iPP blend melts, which might be highly effective on enhancing nucleation rate of

iPP in the surface of PET microfibers. Jay et al. [41] suggested that in a polymer undergoing a shear flow on a macroscopic scale, the deposit of a chain segment on the surface of the solid layer at a microscopic level can change the flow to a local elongational flow, which affects

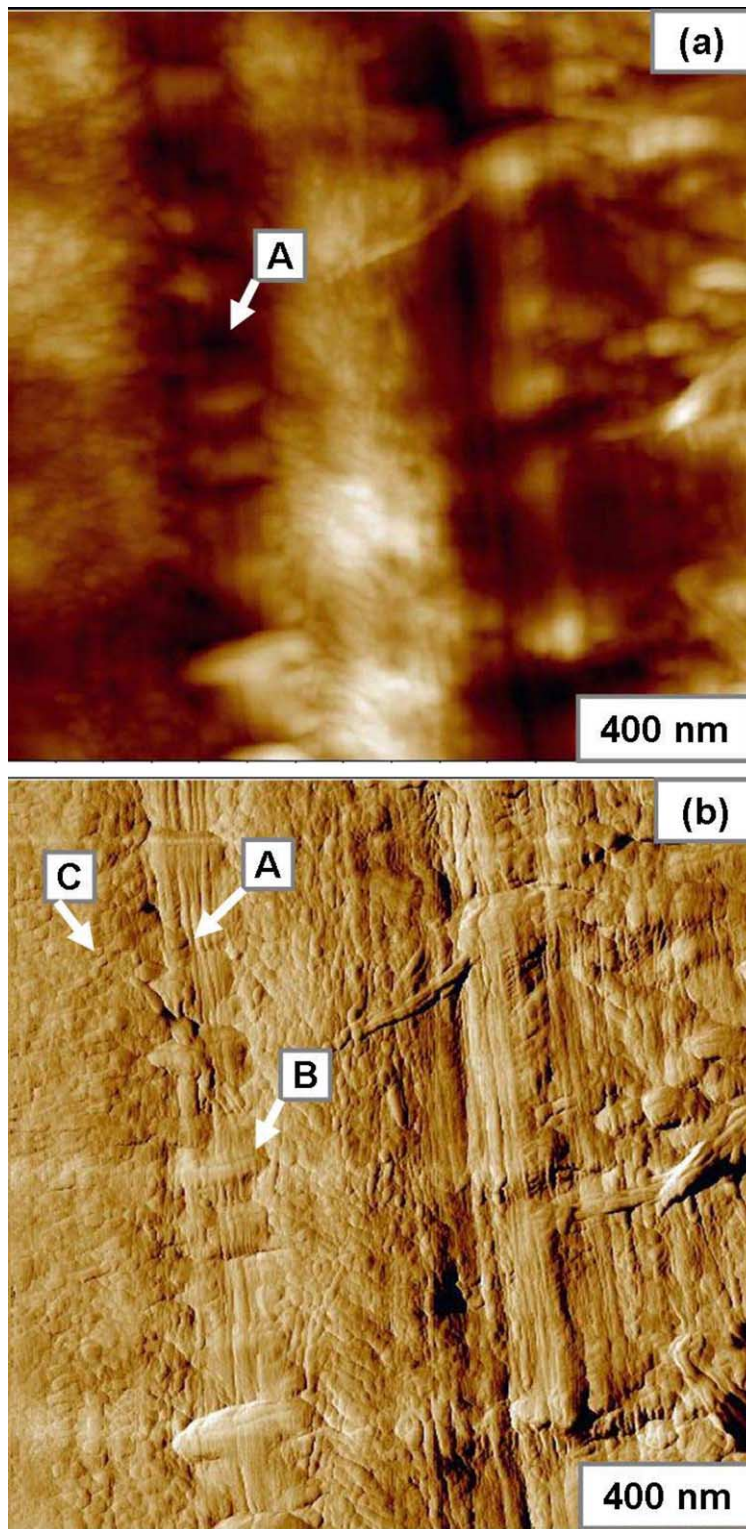


Fig. 7. AFM images of the cryogenic cut surfaces of the as-stretched microfibrillar PET/iPP (15/85 by weight) blend showing the transcrystalline layers and the shish-kebab structure. (a) Height images; (b) phase images. A, B and C inside the images represent the shish of iPP, the kebab of iPP induced by iPP shish, and the kebab of iPP induced by PET microfibers, respectively.

crystallization more than the shear. Such mechanisms were found to be effective in montmorillonite (MMT)/iPP nanocomposites as well [42]. While exfoliated particles interact with polymer chains on their surface, intercalated particles might be surrounded by fragments of chains, which are partially introduced and immobilized between clay nanolayers. Orientation of those chains might play an important role in nucleation of crystallization under shear. Moreover, the additional effect of MMT layers was considered to be the orientation of clay platelets during the flow promoting the orientation of macromolecules. In the present study, the combination of both microfibers and flow field is, therefore, not a simple adding-up. iPP melt in fact flows in a solid network formed by the PET microfibers, which is expected to produce higher stretch and local shear strength on the molecular chains of iPP. The row structures often occur near the surfaces of PET microfibers. This gives another interesting point on the formation of iPP nuclei. Three kinds of nucleation origins can be expected in our case: (1) the classical row-nuclei model, which generally occurs in flow-induced crystallization in a simple super-cooled polymer melt [43], (2) fiber nuclei model [19,44], which can also take place under quiescent condition, (3) nuclei induced fiber assistant alignment. In the third case, the fibers help the alignment of matrix molecular chains, which subsequently form the nuclei. Here the crystals do not grow from the fiber (like in the second model), but from a thin layer of matrix molecules. In fact, the third micro-nucleation model is also supported by its macroscopic counterpart. During shear-induced crystallization, a thin polymer layer near the wall of shearing cell always shows birefringence immediately after the application of a step shear [37]. The presence of a surface induces rheological heterogeneity and promotes the alignment of molecular chains and primary nucleation. Based on third model, we can also explain why some fibers can induce transcrystallites under flow field rather than at quiescent condition. It hardly image that a flow field can change the surface properties of the organic or inorganic fibers. However, it is understandable that polymer molecular chains tend to align with the same orientation as the fibers under an elongational flow. The nuclei are the combination of fiber and flow field induced thin row structures rather than the original fibers. This difference may not be distinguished by normal POM and SEM techniques.

The morphological observation of the shear-induced crystallized sample can help to acquire some evidences of the nucleation mechanisms proposed above. Unfortunately, due to a very strong adhesion of all samples to quartz glasses it was not possible to remove samples after crystallization from shear apparatus and to study them by other methods like SEM, transmission electronic microscope (TEM), and AFM, etc. Essentially, shear and elongational flows have a similar effect on the crystallization kinetics and crystal morphology of a semi-crystalline polymer, but the latter is more effective [39,40,45,46]. For example, both can induce

nucleus and crystalline morphology like shish-kebab. The as-hot stretched sample has experienced a combined shear and elongational flow field during processing, and in the samples, the solid PET microfibers existed during iPP crystallization since PET phase has a higher crystallization temperature than iPP. Therefore, there is more or less similarity between the as-hot stretched sample and the shear-induced crystallized ones. Based on this, we examine the morphology of the as-hot stretched sample by AFM, as shown in Fig. 7. It is found that hardly any fibers exist on the surface. Instead, a large number of straight slots are exposed on the surface (Fig. 7(a), region A), which is due to the scratching out of PET fibers during the cutting process. A typical row nucleus is revealed at the bottom of the slot (Fig. 7(b), region A), which threads many kinks (region B). This kind of morphology, termed shish-kebab, can be found in normal shear or elongational flow induced crystallization. In addition, thinner lamellar crystals, which are transcrystalline layers, pack around the slot, nearly perpendicular to the flow direction (region C). The deviation from the exactly perpendicular direction is possibly induced by deformation during hot stretching. Considering the proposed nucleation mechanisms, one can assign the shish-kebab to shear nucleus and the microfiber assistant nucleus, while the transcrystalline layers to the microfiber nucleus.

4. Conclusions

A well-defined in situ microfibrillar structure in PET/iPP blend was generated by a slit die extrusion, hot stretching, and quenching process. The on-line SAXS results show that PET microfibers have high nucleation for iPP crystallization. The shear-induced crystallization for iPP was also observed. Three nucleation origins are proposed in microfibrillar reinforced blends under shear flow field: (a) the classical row nuclei model, (b) fiber nuclei and (c) nuclei induced by fiber assistant alignment. The last model provides a natural explanation for the case that an oriented structure only occurs in some microfiber reinforced blends under the flow rather than without the external field. Moreover, the neat iPP forms common spherulites, while the diluted microfibrillar blend with 1 wt% of PET has a typical transcrystalline structure, when they experience a non-isothermal crystallization at a cooling rate of 10 °C/min from 200 °C to room temperature.

Acknowledgements

The authors gratefully acknowledge the financial support of this work by the Sichuan Youth Science and Technology Foundation (Contract Number: 04ZQ026-037).

References

- [1] Evstatiev M, Fakirov S, Friedrich K. In: Paul DR, Meyer A, Bucknall CB, editors. *Polymer blends. Performance*, vol. 2. New York: Wiley; 1999. p. 455.
- [2] Fakirov S, Evstatiev M, Petrovich S. *Macromolecules* 1993;26: 5219–26.
- [3] Fakirov S, Evstatiev M. *Adv Mater* 1994;6:395–8.
- [4] Evstatiev M, Fakirov S, Krasteva B, Friedrich K, Covas JA, Cunha AM. *Polym Eng Sci* 2002;42:826–35.
- [5] Li ZM, Yang MB, Xie BH, Feng JM, Huang R. *Polym Eng Sci* 2003; 43:615–28.
- [6] Li ZM, Yang W, Huang R, Fang XP, Yang MB. *Macromol Mater Eng* 2004;289:426–52.
- [7] Huson MG, McGill WJ. *J Polym Sci, Polym Phys Ed* 1985;23:121–8.
- [8] Avalos F, Lopez-Manchado MA, Arroyo M. *Polymer* 1998;39: 6173–8.
- [9] Saujanya C, Radhakrishnan S. *Polymer* 2001;42:4537–48.
- [10] Bogoeva-Gaceva G, Janevski A, Grozdanov A. *J Appl Polym Sci* 1998;67:395–404.
- [11] Nishida K, Konishi T, Kanaya T, Kaji K. *Polymer* 2004;45:1433–7.
- [12] Silvestrea C, Cimmino S, Pirozzi B. *Polymer* 2003;44:4273–81.
- [13] Cho K, Saheb DN, Yang H, Kang BI, Kim J, Lee SS. *Polymer* 2003; 44:4053–9.
- [14] Agarwal PK, Somani RH, Weng WQ, Mehta A, Yang L, Ran SF, et al. *Macromolecules* 2003;36:5226–35.
- [15] Mendoza RG, Regniera G, Seiler W, Lebrun JL. *Polymer* 2003;44: 3363–73.
- [16] Li ZM, Yang MB, Xie BH, Feng JM, Huang R. *Polym Eng Sci* 2002; 43:615–28.
- [17] Li ZM, Yang W, Li LB, Xie BH, Huang R, Yang MB. *J Polym Sci, Part B: Polym Phys* 2004;42:374–85.
- [18] Li ZM, Li LB, Shen KZ, Yang MB, Huang R. *J Polym Sci, Part B: Polym Phys* 2004;42:4095–106.
- [19] Li ZM, Lu A, Lu ZY, Shen KZ, Li LB, Yang MB. *J Macromol Sci, Part B: Phys* 2005;44:203–16.
- [20] Li ZM, Li LB, Shen KZ, Yang W, Huang R, Yang MB. *Macromol Rapid Commun* 2004;25:553–7.
- [21] Li LB, de Jeu WH. *Macromolecules* 2003;36:4862–7.
- [22] Wilkinson AN, Ryan AJ. *Polymer processing and structure development*. Dordrecht: Kluwer; 1998.
- [23] Toki S, Sics I, Ran SF, Liu LZ, Hsiao BS, Murakami S, et al. *Macromolecules* 2002;35:6578–84.
- [24] Somani RH, Hsiao BS, Nogales A, Srinivas S, Tsou AH, Sics I, et al. *Macromolecules* 2000;33:9385–94.
- [25] Avalos F, Lopez-Manchado MA, Arroyo M. *Polymer* 1998;39: 6173–8.
- [26] Torre FJ, Cortazar MM, Gomez MA, Ellis G, Marco C. *Polymer* 2003; 44:5209–17.
- [27] Liu JC, Li HH, Duan YX, Jiang SD, Miao ZJ, Wang JJ, et al. *Polymer* 2003;44:5423–8.
- [28] Li HH, Zhang XQ, Duan YX, Wang DJ, Li L, Yan SK. *Polymer* 2004; 45:8059–65.
- [29] Loos J, Schimanski T, Hofman J, Peijs T, Lemstra PJ. *Polymer* 2001; 41:3827–34.
- [30] Abuzaina FM, Fitz BD, Andjelic S, Jamiolkowski DD. *Polymer* 2003; 43:4699–708.
- [31] Ran SF, Hsiao BS, Agarwal PK, Varma-Nair M. *Polymer* 2003;44: 2385–92.
- [32] Varga J, Karger-Kocsis J. *J Polym Sci, Part B: Polym Phys* 1996;34: 657.
- [33] Pogodina NV, Siddiquee SK, van Egmond JW, Winter HH. *Macromolecules* 1999;32:1167–74.
- [34] Somani RH, Hsiao BS, Nogales A, Srinivas S, Tsou AH, Balta-Calleja F, et al. *Macromolecules* 2001;34:5902–9.
- [35] Li LB, de Jeu WH. *Phys Rev Lett* 2004;92:075506–075501-3.
- [36] Somani RH, Yang L, Hsiao BS, Agarwal PK, Fruitwala HA, Tsou AH. *Macromolecules* 2002;35:9096–104.
- [37] Seki M, Thurman DW, Oberhauser JP, Kornfield JA. *Macromolecules* 2002;35:2583–94.
- [38] Eisenriegler E. *Polymers near surface*. London: World Scientific; 1993.
- [39] Yamazaki S, Watanabe K, Okada K, Yamada K, Tagashira K, Toda A, et al. *Polymer* 2005;46:1675–84.
- [40] Yamazaki S, Watanabe K, Okada K, Yamada K, Tagashira K, Toda A, et al. *Polymer* 2005;46:1685–92.
- [41] Jay F, Haudin JM, Monasse B. *J Mater Sci* 1999;34:2089.
- [42] Nowacki R, Monasse B, Piorowska E, Galeski A, Haudin JM. *Polymer* 2004;45:4877–92.
- [43] Somani RH, Hsiao BS, Nogales A, Srinivas S, Tsou AH, Sics I, et al. *Macromolecules* 2000;33:9385–94.
- [44] Ishida H, Bussi P. *Macromolecules* 1991;24:3569–77.
- [45] Keller A, Odell JA. *Colloid Polym Sci* 1985;263:181–201.
- [46] Dukovski I, Muthukumar M. *J Chem Phys* 2003;118:6648–55.